Bull. Mater. Sci., Vol. 39, No. 5, September 2016, pp. 1263–1272. © Indian Academy of Sciences.
DOI 10.1007/s12034-016-1268-x

Microstructure and oxidation behaviour of TiAl(Nb)/Ti_2AlC composites fabricated by mechanical alloying and hot pressing

HADI KARIMI, ALI GHASEMI* and MORTEZA HADI
Materials Engineering Department, Malek Ashtar University of Technology, Shahin Shahr 83145/115, Iran

MS received 6 January 2016; accepted 23 February 2016

Abstract. **TiAl-based intermetallic matrix composites with dispersed Ti_2AlC particles and different amounts of Nb were successfully synthesized by mechanical alloying and hot pressing. The phase evolution of Ti–48 at%. Al elemental powder mixture milled for different times with hexane as a process control agent was investigated. It was found that after milling for 25 h, a Ti(Al) solid solution was formed; also with increase in the milling time to 50 h, an amorphous phase was detected. Formation of a supersaturated Ti(Al) solid solution after 75 h milling was achieved by crystallization of amorphous phase. Addition of Nb to system also exhibited a supersaturated Ti(Al,Nb) solid solution after milling for 75 h, implying that the Al and Nb elements were dissolved in the Ti lattice in a non-equilibrium state. Annealing of 75 h milled powders resulted in the formation of equilibrium TiAl intermetallic with Ti_2AlC phases that showed the carbon that originates from hexane, participated in the reaction to form Ti_2AlC during heating. Consolidation of milled powder with different amounts of Nb was performed by hot pressing at 1000°C for 1 h. Only the presence of γ-TiAl and Ti_2AlC was detected and no secondary phases were observed on the base of Nb. Displacement of γ-TiAl peaks with Nb addition implied that the Nb element was dissolved into TiAl matrix in the form of solid solution, causing the lattice tetragonality of TiAl to increase slightly. The values for density and porosity of samples indicated that condition of hot pressing process with temperature and pressure was adequate to consolidate almost fully densified samples. The isothermal oxidation test was carried out at 1000°C in air to assess the effect of Nb addition on the oxidation behaviour of TiAl/Ti_2AlC composites. The oxidation resistance of composites was improved with the increase in the Nb content due to the suppression of TiO_2 growth, the formation and stabilization of nitride in the oxide scale and better scale spallation resistance.**

Keywords. **Mechanical alloying; TiAl intermetallic; oxidation.**

1. Introduction

Alloys based on the γ-TiAl intermetallic have attracted considerable attention over the past few decades because of their excellent properties such as low density, high melting point, high modules, high strength and relatively good properties at elevated temperatures [1,2]. Because of these properties, they have the great potential to be used for specific applications in the aerospace and automotive industries. Replacement of nickel-based super alloy parts in gas turbine engines is one of the foremost applications considered for titanium aluminides. Producing parts made of titanium aluminides in gas turbine engines such as turbine blade is expected to decrease the structural weight of engines by 20–30% [3,4]. However, apart from these supreme properties, low ductility and poor fracture toughness at room temperature and insufficient strength and oxidation resistance at high temperatures limited their practical applications. Not forming a protective Al_2O_3 layer at high temperatures in air, led to low oxidation resistance above 800°C which is one of the major obstacles should be solved to utilize TiAl alloys [5,6].

Various techniques have been devised to improve properties of TiAl alloys at room and elevated temperatures. Addition of alloying elements such as Nb, Cr, V, Mn, W, Si, C and others has been effectively applied to improve their shortcomings [7–9]. Among these elements, Nb is one of the most important additives that can significantly enhance the high temperature strength and also oxidation and creep resistance [10,11]. On the other hand, it has been reported that ductility of these alloys can be improved by grain refinement [12]. Mechanical alloying (MA) with subsequent consolidation processes can prepare titanium aluminides compacts with ultra-fine grains in the sub-micron to nanometer range [13]. Therefore, TiAl alloys produced by this route are expected to provide better workability and ductility at room temperature [14,15]. In addition, most challenges related to ingot metallurgy such as macro-segregations and central porosity can be tackled [16]. Fabrication of TiAl matrix composites is another way that applied to improve their properties successfully. According to the type of particle reinforcement used, ductility and toughness at ambient temperatures and also high-temperature strength, oxidation and creep resistance can be improved [17,18]. A number of TiAl matrix composites have been developed with different particle reinforcements such as Al_2O_3, TiB_2, Ti_5Si_3, Si_3N_4, SiC,

*Author for correspondence (ali13912001@yahoo.com)

Ti_2AlN and Ti_2AlC that can be used for different purposes [19–24]. Among them, Ti_2AlC has been considered as a beneficial particle because of the unusual combination of useful and unique properties like excellent machinability, thermal shock resistance, low density, good thermal and electrical conductivities and high-temperature oxidation resistance, which make it to exhibit both ceramic and metallic properties. In addition, density and thermal expansion coefficient of the Ti_2AlC and TiAl phases are close to each other, so that all these benefits make the Ti_2AlC particles a superior candidate to be introduced into the TiAl matrix [25,26]. TiAl matrix composites have been already fabricated by mechanical alloying and subsequent heat treatment successfully by several groups of researchers [27–29]. The use of process control agents (PCAs) during milling increases the effectiveness of milling by decreasing powder agglomeration and also applying it to introduce new elements into the alloy. Carbon from the decomposition of hexane can lead to the formation of carbide during milling and further heating as reported earlier [30,31]. In the present study, the idea of improving properties of TiAl alloys with several methods simultaneously was used to fabricate TiAl matrix composites with and without the addition of Nb by mechanical alloying and hot press consolidation. Phase evolutions during the milling in hexane and further heat treatment were investigated. The effect of Nb addition on phases and microstructure and also high temperature oxidation behaviour of bulk samples were studied.

2. Experimental

Powders of titanium (>98.5% pure, average particle size of 50 μm), aluminum (99% pure, average particle size of 100 μm) and niobium (99.8% pure, average particle size of 70 μm) were used as starting materials. The powders were initially mixed to the compositions according to table 1. The mixtures were mechanically alloyed at a room temperature in a planetary-type ball mill with a tungsten carbide (WC) vial and WC balls at a rotation speed of 300 rpm. The milling was performed for several periods varying from 0 to 75 h with the addition of hexane as a process control agent. The ball to powder weight ratio (BPR) was 10:1 and 13 with a diameter of 10 mm were used. Heat treatment of milled powders was done in a tube furnace for 1 h at various temperatures under a high purity argon atmosphere. The milled powders were hot pressed under 30 MPa for 1 h at 1000°C in a graphite mould coated with boron nitride (BN) inside vacuum (10^{-3} torr).

Table 1. Powder compositions (at%) of fabricated samples.

	Ti	Al	Nb
Alloy 1	52	48	0
Alloy 2	50	48	2
Alloy 3	48	48	4
Alloy 4	46	48	6
Alloy 5	44	48	8

A resistance furnace with the heating rate of about 20°C min^{-1} was used.

Isothermal oxidation tests were performed at 1000°C in static laboratory air for 10 h. For oxidation tests, the hot-pressed (HPed) samples were cut into rectangular specimens with dimensions of 10 × 10 × 1 mm^3. The specimens were ground successively to 1500-grit SiC papers and cleaned with acetone. Isothermal oxidation tests were carried out in a furnace equipped with an electronic balance and in conjunction with a computer to record continuous mass variation as a function of time. The accuracy of the used balance was 0.01 mg.

Phase identification of powders and HPed samples and also oxide scales were conducted by X-ray diffraction (XRD) method using a Philips PW-3040 with CuKα radiation operating at a voltage of 40 kV and a current of 30 mA. The Scherrer formula was used to estimate the crystallite size from broadening of XRD peaks [32]:

$$d = 0.9\lambda/\beta\cos\theta, \quad (1)$$

where d is the mean crystallite size, β the full width at half maximum (FWHM), θ the diffraction angles and λ the wavelength of X-ray.

The microstructure was studied by scanning electron microscopy (SEM, VEGA Tescan machine) equipped with an energy-dispersive spectrometer (EDS) for the semi-quantitative investigation. Density and porosity measurements of the HPed samples were measured using Archimedes principle.

3. Results and discussion

3.1 *Mechanical alloying process*

3.1a *X-ray diffraction analysis of Ti–48Al*: To study the structure evolution during MA, Ti–48Al powder mixture was mechanically alloyed for 25, 50 and 75 h. Figure 1 shows the XRD patterns of Ti–48Al after different milling times. After 25 h milling, the peaks corresponding to pure Al (cubic; ref. ICDD code: 01-085-1327) and Ti (hexagonal; ref. ICDD code: 00-044-1294) were observed, but the peaks intensity was decreased and their broadening was increased because of the reduction of grain size and the enhancement of lattice strain during MA. In addition, the peaks of Ti were shifted to the higher angles, showing the formation of Ti(Al) solid solution. To compare the amount of displacement of Ti peaks during MA, the 2θ locations of Ti diffraction peaks at different milling times are listed in table 2. Due to the smaller atomic radius of aluminum, as compared to titanium, during MA, Al atoms were diffused to Ti lattice and as a result, interplaner spacing of Ti crystal structure was reduced according to Bragg's law, which predicts the increase of diffraction angles. By considering Ti–Al phase diagram [3], it can be seen that solubility of Al in Ti is remarkable, but solubility of Ti in Al is limited at different temperatures. It can be expected that Al is diffused into Ti essentially during MA. The presence of a broadpeak in the XRD pattern with

increasing time to 50 h indicates that an amorphous phase was obtained. Amorphization during MA is believed to occur by increasing the free energy of system. The accumulation of structural defects and the increase in grain boundary area as a result of the decrease in grain size would contribute to the increase in free energy of the system [30]. By increasing milling time to 75 h, a crystalline phase was formed due to crystallization of amorphous phase. The peaks position of this new phase corresponds to supersaturated Ti(Al) solid solution, indicating that powders possess a crystal structure of Ti at this time of milling. MA as a non-equilibrium processing technique can attain a significant increase in solid solubility limit and it is expected to increase with milling time as diffusion progresses and reaches a supersaturation level. The presence of peaks corresponding to hexagonal Ti and the disappearance of the Al peaks suggest that during MA, Al has been dissolved in Ti lattice and a supersaturated solid solution hcp–Ti(Al) has been formed. The crystallite size value of Ti element after 25 and 75 h milling times was calculated by using Scherer equation that reached 23 and 11 nm, respectively.

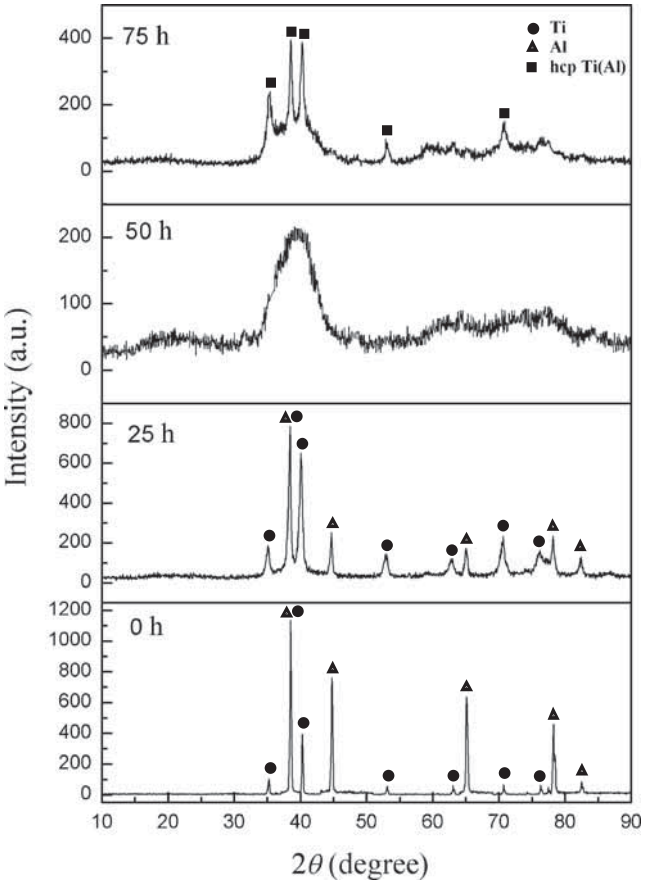

Figure 1. XRD patterns of Ti–48Al milled for different times.

Table 2. The 2θ locations of peaks corresponding to Ti according to XRD patterns for Ti–48Al powder at different milling times.

Milling time (h)	2θ°	2θ°	2θ°
0	35.16	38.44	40.06
25	35.20	38.47	40.19
75	35.26	38.53	40.31

3.1b *X-ray diffraction analysis of Ti–48Al–xNb*: XRD patterns of the samples with different contents of the Nb mechanically alloyed for 75 h are shown in figure 2. By comparing the diffraction patterns for TiAl and TiAl–xNb milled for 75 h in figures 1 and 2, it can be seen that the patterns of samples with different added amounts of Nb were almost identical in peak position and peak appearance. This result indicates that the crystalline structure of the powders is basically the same as Ti structure retained and other elements such as Al and Nb are dissolved in the Ti lattice. Due to the disappearance of Al and Nb peaks and broadening and weakening of Ti peaks, it can be concluded that a supersaturated Ti(Al,Nb) solid solution with a very fine grain size has been obtained. More displacement of Ti peaks for samples with Nb addition in XRD pattern was compared with Ti–48Al to show that not only major Al, but also Nb was dissolved in the Ti lattice, as shown in table 3. The crystallite size values for samples after 75 h milling time are listed in table 4, indicating that for all the samples, they are in the range of 10–12 nm.

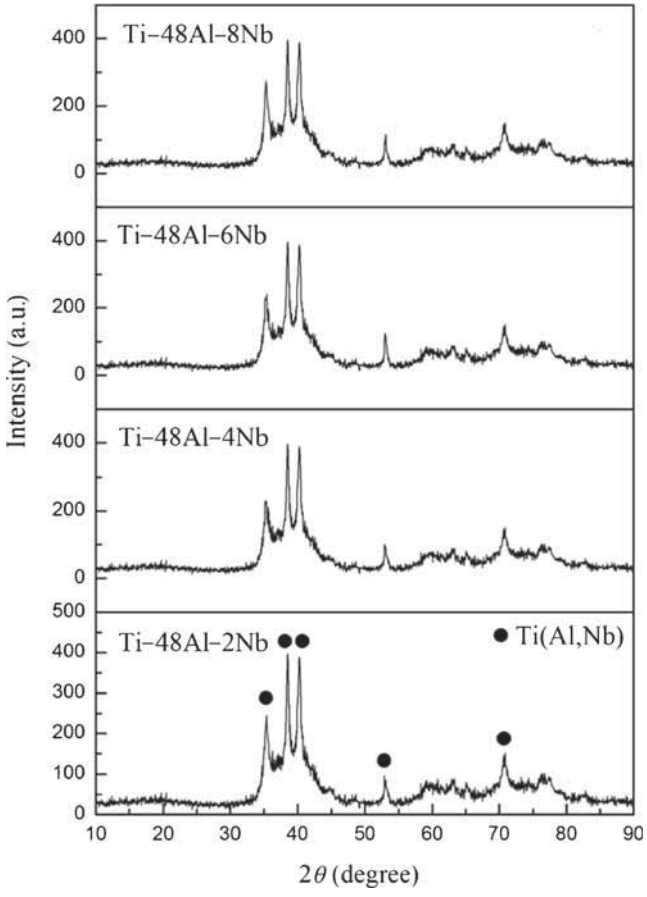

Figure 2. XRD patterns of Ti–48Al–xNb milled for 75 h.

3.1c *Microstructural evaluation*: The morphology of Ti–48Al–xNb powders mechanically alloyed for 75 h was studied by SEM analysis as shown in figure 3. It can be seen that irregular shaped particles obtained for all the samples and heavy deformation were introduced into the particles. Moreover, a broad range of particle size distribution was observed. It varied from 200 nm to 10 μm. Reducing the particle size of the powder in the range of submicron scale might

Table 3. The 2θ locations of peaks corresponding to Ti according to XRD patterns for Ti–48Al–xNb powders milled for 75 h.

Sample	$2\theta°$	$2\theta°$	$2\theta°$
Ti–48Al–2Nb	35.27	38.54	40.33
Ti–48Al–4Nb	35.28	38.56	40.34
Ti–48Al–6Nb	35.30	38.57	40.37
Ti–48Al–8Nb	35.31	38.59	40.38

Table 4. The crystallite size of Ti–48Al–xNb powders milled for 75 h.

Sample	Crystallite size (nm)
Ti–48Al–2Nb	11
Ti–48Al–4Nb	10.5
Ti–48Al–6Nb	12
Ti–48Al–8Nb	11

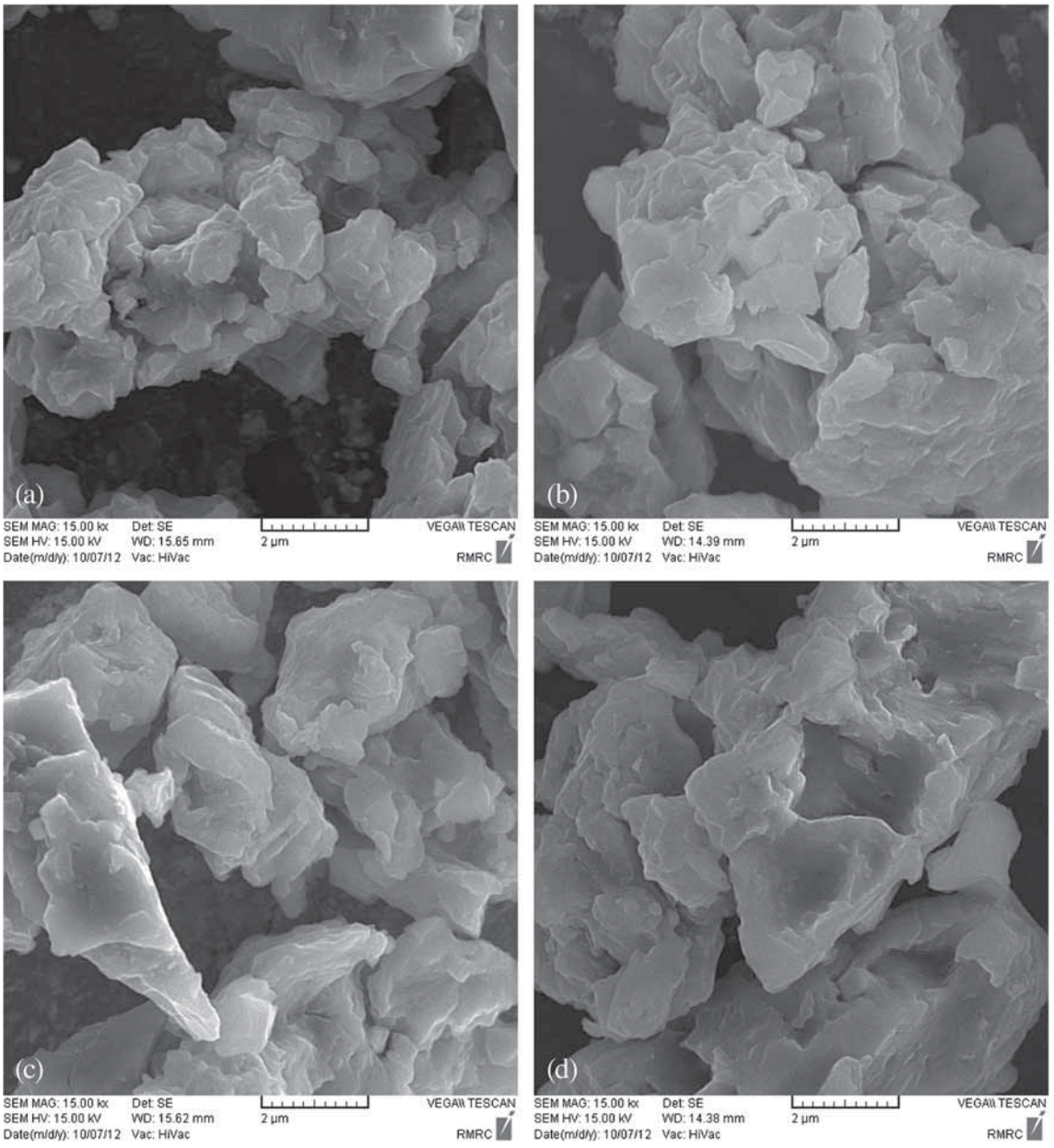

Figure 3. SEM images of Ti–48Al–xNb particles milled for 75 h: (**a**) Ti–48Al–2Nb, (**b**) Ti–48Al–4Nb, (**c**) Ti–48Al–6Nb and (**d**) Ti–48Al–8Nb.

be attributed to the presence of brittle titanium powders. During milling, the brittle components get fragmented and their particle size is continuously reduced. Many agglomerates were also observed, indicating the adhesion of much smaller particles to each other. Size enlargement through agglomeration was intensive for particles in the range of submicrons, making it difficult to determine the exact size of particles.

3.1d *Annealing process*: Figure 4 shows the XRD patterns of Ti–48Al powders mechanically alloyed for 75 h after annealing at different temperatures. In the XRD pattern obtained by heating the powder to 600°C, no transformation occurred and peaks of supersaturated Ti(Al) solid solution with hcp structure were still detectable. By heating at 800°C, the presence of the Ti(Al), Ti_2AlC (hexagonal; ref. ICDD code: 00-029-0095) and metastable fcc TiAl phases could be seen in the XRD pattern; truly at this temperature, the transformation of Ti(Al) to TiAl($L1_0$) also started. Because of coherency between fcc TiAl phase and Ti(Al) phase with hcp structure, the formation of TiAl($L1_0$) proceeded through intermediate fcc TiAl phase. Ti_2AlC phase was also formed at this temperature and its intensity was high. Carbon from the decomposition of the hexane used as a PCA in this study participated in the reaction to form Ti_2AlC during heating. Since hexane is an organic compound with a low boiling point (between 50 and 70°C), it is decomposed during milling according to raise in the temperature as the kinetic energy of the grinding medium leads to introduction of carbon into the system. Carbon reacts with the powders and forms carbides which can be uniformly dispersed in the matrix. As shown by the XRD pattern, equilibrium TiAl ($L1_0$) (tetragonal; ref. ICDD code: 00-005-0678) and Ti_2AlC phases are obtained by increasing the temperature to 1000°C. The peaks corresponding to Ti(Al) phase were not observed at this temperature and the metastable fcc TiAl phase was completely transformed into TiAl($L1_0$) phase; in fact, stable phase structure was obtained. Transition of the fcc into $L1_0$ phase was occurred with tetragonal distortion that resulted in splitting diffraction lines such as $(200)_{fcc} \rightarrow (002)(200)_{L1_0}$ and $(220)_{fcc} \rightarrow (202)(220)_{L1_0}$, as pointed out

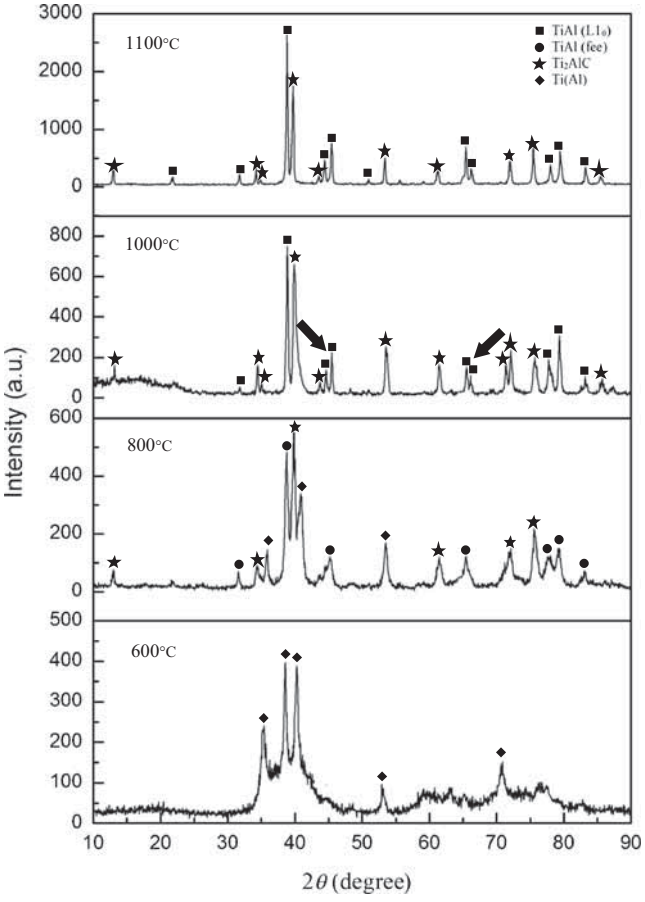

Figure 4. XRD patterns of Ti–48Al powders mechanically alloyed for 75 h after annealing at different temperatures.

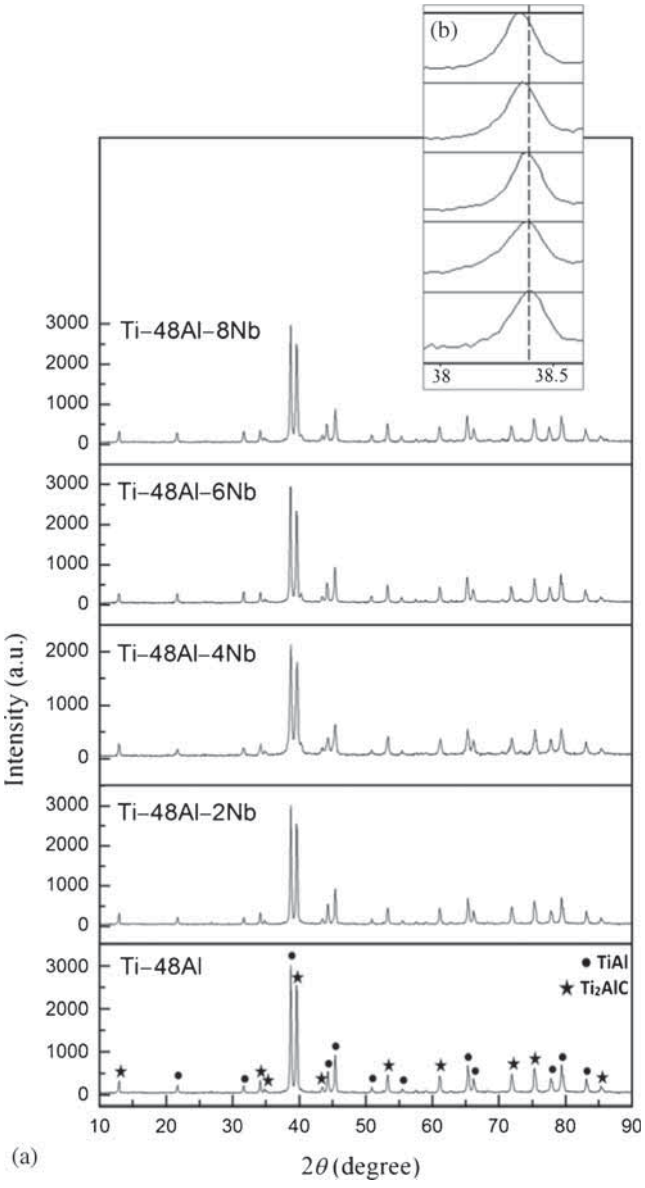

Figure 5. (**a**) XRD patterns of the bulk samples with different amounts of Nb and (**b**) displacement of TiAl peak to lower angles.

by the arrow (figure 4). This is in agreement with previous works reported by others [33,34]. By increasing the temperature from 1000 to 1100°C, no new transformation occurred and diffraction peaks for TiAl and Ti_2AlC phases were detected as shown by the XRD pattern; it can be seen that intensities of the phases were increased and peak widths of them were decreased. This change in the pattern was due to the reduction in lattice strain and increasing crystallite size.

3.2 *Hot press processes*

3.2a *X-ray diffraction analysis*: The results in the previous section indicated that the TiAl/Ti_2AlC composite could be fabricated by heating the milled powder to 1000°C and more. Synthesizing ultra-fine grained alloys needs to prevent grain growth during heating as coarsening of grain occurred quickly at temperatures greater than 1000°C; thus, the temperature for hot pressing (HP) process was determined to be 1000°C.

Figure 5a shows the XRD patterns of the bulk samples with different amounts of Nb produced by HP of the 75 h milled powder at 1000°C for 1 h. It can be found that in the patterns, all the samples consisted of γ-TiAl and Ti_2AlC phases and no oxides, carbides or other phases on the base of Nb were detected. The phase composition of TiAl/Ti_2AlC composites were unaffected by the addition of Nb element and patterns for all the samples were almost the same. Addition of elements to TiAl changed the volume and c/a ratio of γ-TiAl. These changes depend on sublattice site that added the occupied elements. The c/a ratio of the lattice is increased

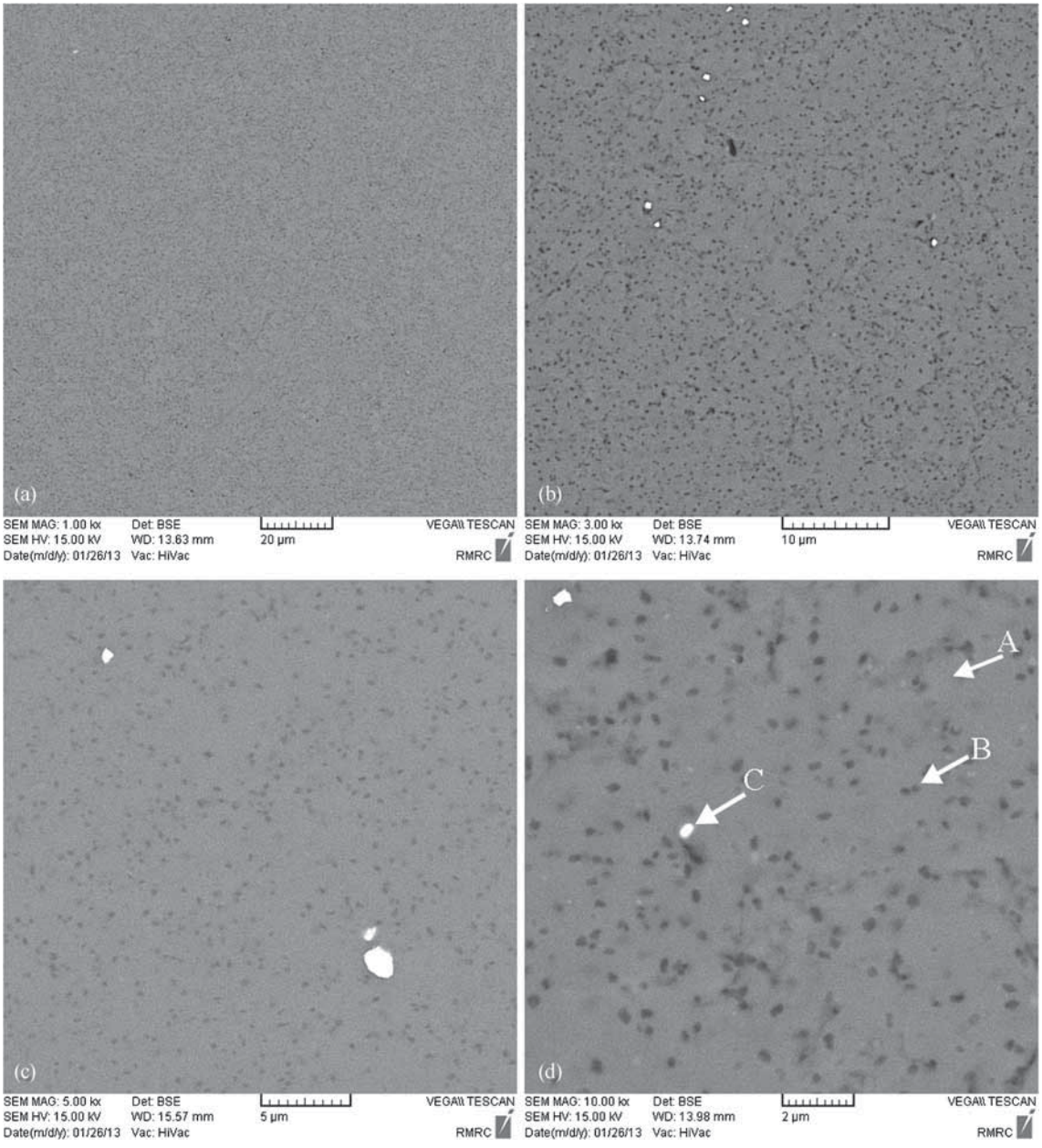

Figure 6. Backscattered scanning electron microscopic (BSE) images of the polished surfaces of bulk TiAl(2Nb)/Ti_2AlC composite at different magnifications.

if elements are substituted for Ti. As Nb atoms prefer the Ti-sites, it can be expected that c/a ratio would be increased [35]. Figure 5b shows the peak position of the TiAl with different amounts of Nb. The shift of peaks corresponding to (111) plane towards the lower angles demonstrates an increase in the lattice parameters of the TiAl matrix. Further displacement of peaks by the increase in the Nb content implies that Nb element is dissolved in TiAl matrix in the form of solid solution. Broadening of the XRD peaks indicates that grain sizes of HPed samples are very small. The crystallite size values of all the samples are in the range of 45–50 nm.

3.2b *Microstructural evaluation*: Figure 6 shows the backscattered SEM images of the polished surfaces of bulk TiAl(2Nb)/Ti_2AlC composites at different magnifications. Three types of contrast include gray, black and white identified on the images. According to the results of EDS point scan on figure 7 and the contents of Ti and Al in different contrasts, it is reasonable to relate the gray contrast to TiAl phase and black contrast to Ti_2AlC phase. This is in good agreement with XRD identification. Also white contrast is in accordance with tungsten (W) i.e., related to the contamination of the powders by using tungsten carbide balls and vial. As a result, this alloy consists of TiAl as matrix and Ti_2AlC as reinforcement particles that are round shaped and uniformly dispersed in the matrix. Also, the EDS results revealed the presence of high concentration of Nb in the matrix than in the reinforcement. This indicates that Nb has been in the form of solid solution in the TiAl matrix. The phases and distribution for all samples are similar. The density and amount of porosities, which were measured by the method of Archimedes, are presented in table 5. It can be seen that the density of TiAl/Ti_2AlC composites has been increased obviously with the addition of Nb because the atomic mass of Nb is greater than Ti. Addition of Nb instead of Ti, increases the densities. The values for density and porosity indicate that the samples were almost fully densified and the amount of porosity was very low. Ultrafine particles with the higher surface area have high energy and by providing shorter diffusion distances, they are able to increase atomic diffusion across the

Table 5. The values of density and porosity for TiAlxNb/Ti_2AlC composites.

Nb (at%)	Density (g cm^{-3})	Porosity (%)
0	3.89	1.2
2	3.92	1.4
4	3.96	1.3
6	4.01	1.5
8	4.04	1.5

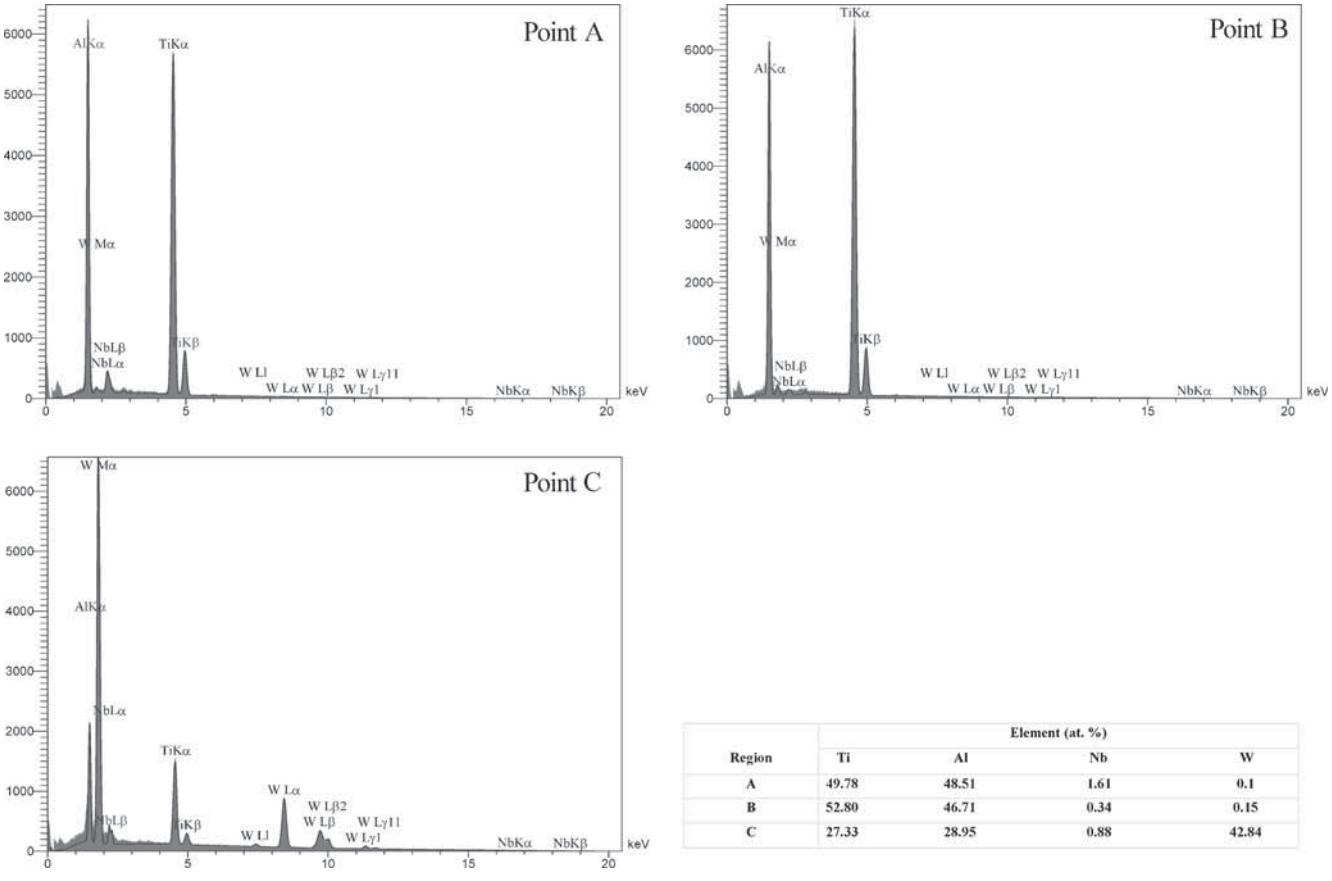

Region	Element (at. %)			
	Ti	Al	Nb	W
A	49.78	48.51	1.61	0.1
B	52.80	46.71	0.34	0.15
C	27.33	28.95	0.88	42.84

Figure 7. Results of EDS point scan on different regions on figure 6d.

boundaries and enhance the number of bonds among the particles. Thus, the higher density and the lower porosity can be obtained with ultrafine particle size. It can be seen from figure 6 that no obvious porosity was observed in the samples.

3.3 *Oxidation kinetics*

Figure 8 shows the curves of isothermal oxidation kinetics of the TiAl(Nb)/Ti_2AlC composites at 1000°C in air. At first, the results for the alloy without Nb addition indicated relatively fast mass gain, but due to the oxide spallation in further oxidation, mass loss occurred clearly and then, by the formation of a more protective oxide scale, a steady state was observed. Because of the poor oxidation resistance of TiAl alloys at 1000°C, oxide spallation during the initial period of the oxidation was observed by other researchers that could divide curve oxidation into several stages [36,37]. From the curve of oxidation, it was clear that the mass change of alloy with the addition of 2% Nb was lower than that of Nb-free alloy. Lower mass gain and mass loss were related to the beneficial effect of Nb on the oxidation resistance of TiAl alloy. Nb with valence +5 acted as a dopant element that reduced oxygen vacancies in rutile lattice owing to the electroneutrality in the oxide that resulted in the suppression of rutile growth [38]. The mass change of alloy with 4% Nb represented a lower mass loss when compared with Nb-free and 2% Nb alloys and at the end, a more protective behaviour was achieved. Also, the slight mass loss of alloy with 6% Nb and the ability to form oxide scale again without spallation indicated a more protective behaviour against oxidation with more Nb addition. By considering the curve for 8% Nb alloys, no spallation was observed and an excellent adherent oxide was formed, contrary to the other alloy. Consequently, the superior oxidation resistance was related to 8% Nb addition by which an oxide scale with good protection effect was established. Figure 9 shows the XRD patterns of specimens isothermally oxidized at 1000°C in air. From the results of XRD pattern for TiAl/Ti_2AlC composite without Nb addition, two oxides of TiO_2 (rutile) (tetragonal; ref. ICDD code: 00-004-0551) and α-Al_2O_3 (corundum) (rhombohedral; ref. ICDD code: 00-001-1296) and also, two phases from the substrate were detected. The high intensity of peaks corresponding to substrate phases in XRD pattern indicated that a thin oxide scale was formed on the surface. The phases detected for 2% Nb alloy were practically identical with Nb-free alloy, but the lower intensity of TiO_2 peaks in 2% Nb alloy confirmed the beneficial role of Nb to suppress rutile growth. For 4% Nb alloy, in addition to oxides and substrates, phases

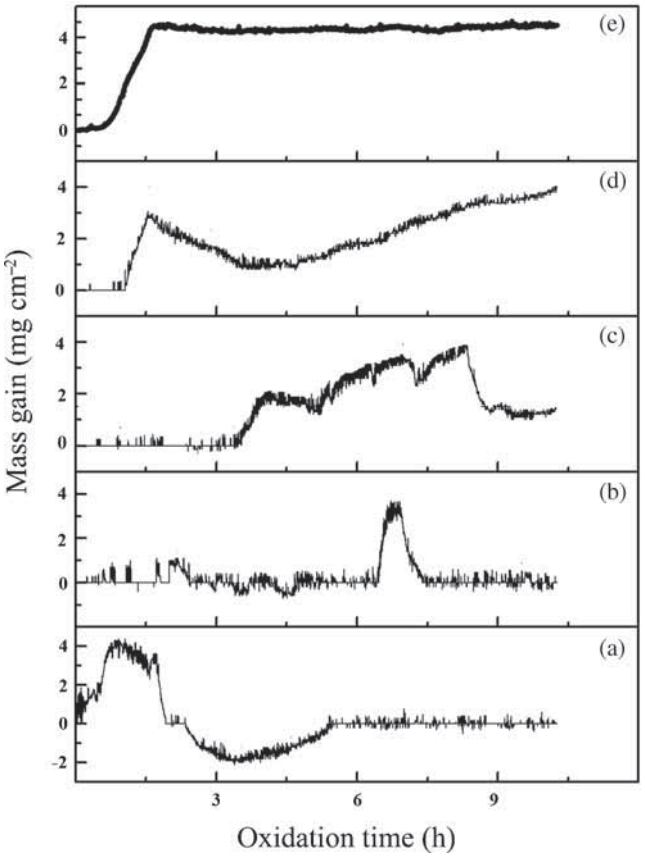

Figure 8. Isothermal oxidation kinetics of TiAl composites at 1000°C in air: (**a**) TiAl/Ti_2AlC, (**b**) TiAl(2Nb)/Ti_2AlC, (**c**) TiAl(4Nb)/Ti_2AlC, (**d**) TiAl(6Nb)/Ti_2AlC and (**e**) TiAl(8Nb)/Ti_2AlC.

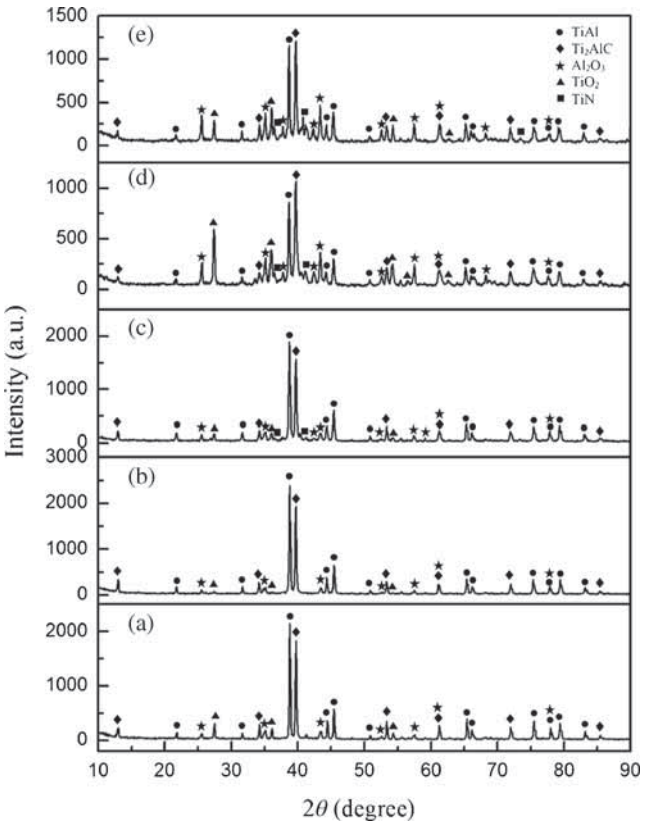

Figure 9. XRD patterns of the TiAl composites isothermally oxidized at 1000°C in air: (**a**) TiAl/Ti_2AlC, (**b**) TiAl(2Nb)/Ti_2AlC, (**c**) TiAl(4Nb)/Ti_2AlC, (**d**) TiAl(6Nb)/Ti_2AlC and (**e**) TiAl(8Nb)/Ti_2AlC.

identified for the two previous alloys, a new nitride phase was detected. By oxidation of TiAl alloy in air, the formation of nitride phases beside oxides was reported [39]. The nitride phases were in the form of TiN or Ti_2AlN that tend to be converted to rutile during oxidation and hampered the formation of a compact protective alumina layer in the scale [40]. The presence of TiN (tetragonal; ref. ICDD code: 00-008-0418) in oxide scale was related to the beneficial effect of Nb to promote the formation and stabilization of TiN which acted as an effective barrier for outward diffusion of metal ions and inward diffusion of oxygen ions. The absence of niobium oxide peaks in the XRD pattern showed that Nb replaced Ti ions in rutile to form $(Ti,Nb)O_2$ in the inner part of the scale. In addition, niobium become enriched at the scale/alloy interface i.e., effective to hinder the diffusion of ions [38]. The only difference between the patterns of 6% and 8% Nb alloys and the previous alloy was the lower intensity of substrate peaks and the higher intensity of oxides peaks, because the oxide scale was quite thicker. Also, the intensity of TiN peaks was enhanced with the increase in Nb content and the intensity of TiO_2 was reduced when compared to Al_2O_3 peaks.

4. Conclusion

Mechanical alloying and hot pressing processes were successfully applied to synthesize TiAl(Nb)/Ti_2AlC composites. Mechanical alloying of elemental Al and Ti powders by using hexane as a PCA led to a different phase transformation. A Ti(Al) solid solution was formed at the 25 h of milling that was transformed to an amorphous phase at 50 h. On further milling, the amorphous phase was transformed to a supersaturated hcp-Ti(Al) solid solution after 75 h of milling. Addition of Nb to system also exhibited a supersaturated Ti(Al,Nb) solid solution after milling for 75 h. It was found that annealing of 75 h milled powders led to the formation of equilibrium TiAl intermetallic with Ti_2AlC phases. The formation of Ti_2AlC was as a result of decomposition of hexane during milling. The bulk TiAl/Ti_2AlC composites with different contents of Nb consolidated by HP process at 1000°C for 1 h showed that peaks position of γ-TiAl was shifted towards lower angles. More displacement of peaks with further Nb addition implied that the Nb element was dissolved into TiAl matrix in the form of solid solution. Characterization of the bulk samples by Archimedes and electron microscopy technique indicated that nearly full density with low porosity was achieved. The oxidation resistance of TiAl/Ti_2AlC composites at 1000°C in air was improved by Nb addition. The effect of Nb on the oxidation resistance was suppression of TiO_2 growth, the formation and stabilization of nitride in the oxide scale and better scale spallation resistance.

References

[1] Wei Z, Yong L, Bin L, Hui-Zhong L and Bei T 2010 *Trans. Nonferrous Met. Soc. China* **20** 547

[2] Liu Q and Nash P 2011 *Intermetallics* **19** 1282

[3] Kothari K, Radhakrishnan R and Wereley N M 2012 *Prog. Aerosp. Sci.* **55** 1

[4] Du H L, Datta P K, Hu D and Wu X 2007 *Corros. Sci.* **49** 2406

[5] Shu S, Qiu F, Xing B, Jin S, Wang Y and Jiang Q 2012 *Intermetallics* **28** 65

[6] Yoshihara M and Kim Y W 2005 *Intermetallics* **13** 952

[7] Chen Y, Niu H, Kong F and Xiao S 2011 *Intermetallics* **19** 1405

[8] Appel F, Christoph U and Oehring M 2002 *Mater. Sci. Eng.* **A329–331** 780

[9] Zhi-Guang L, Yu-Yong C, Li-Hua C, Fan-Tao K and Davies H A 2006 *Trans. Nonferrous Met. Soc. China* **16** 711

[10] Zhang W J and Appel F 2002 *Mater. Sci. Eng.* **A329–331** 649

[11] Lin J P, Zhao L L, Li G Y, Zhang L Q, Song X P, Ye F and Chen G L 2011 *Intermetallics* **19** 131

[12] Farhang M, Kamali A and Nazarian-Samani M 2010 *Mater. Sci. Eng. B* **168** 136

[13] Shu-Long X, Li-Juan X, Yu-Yong C and Hong-Bao Y 2012 *Trans. Nonferrous Met. Soc. China* **22** 1086

[14] Wen-Bin F, Xue-Wen L, Hong-Fei S and Yong-Feng D 2011 *Trans. Nonferrous Met. Soc. China* **21** 333

[15] Bhattacharya P, Bellon P, Averback R S and Hales S J 2004 *J. Alloys Compnd.* **368** 187

[16] Liu B, Liu Y, Zhang W and Huang J S 2011 *Intermetallics* **19** 154

[17] Ramaseshan R, Kakitsuji A, Seshadri S K, Nair N G, Mabuchi H, Tsuda H *et al* 1999 *Intermetallics* **7** 571

[18] Zhu J, Yang W, Yang H and Wang F 2011 *Mater. Sci. Eng. A* **528** 6642

[19] Alamolhoda S, Heshmati-Manesh S and Ataie A 2012 *Adv. Powder Technol.* **23** 343

[20] Niu H Z, Xiao S L, Kong F T, Zhang C J and Chen Y Y 2012 *Mater. Sci. Eng. A* **532** 522

[21] Peng L M, Li Z, Li H, Wang J H and Gong M 2006 *J. Alloys Compnd.* **414** 100

[22] Li Z W, Gao W, Zhang D L and Cai Z H 2004 *Corros. Sci.* **46** 1997

[23] Yeh C L and Shen Y G 2009 *Intermetallics* **17** 169

[24] Mei B and Miyamoto Y 2002 *Mater. Chem. Phys.* **75** 291

[25] Hashimoto S, Nishina N, Hirao K, Zhou Y, Hyuga H, Honda S and Iwamoto Y 2012 *Mater. Res. Bull.* **47** 1164

[26] Shu S, Qiu F, Lü S, Jin S and Jiang Q 2012 *Mater. Sci. Eng. A* **539** 344

[27] Gu D, Wang Z, Shen Y, Li Q and Li Y 2009 *Appl. Surf. Sci.* **255** 9230

[28] Vyas A, Rao K P and Prasad Y V R K 2009 *J. Alloys Compnd.* **475** 252

[29] Yang F, Kong F T, Chen Y Y and Xiao S L 2010 *J. Alloys Compnd.* **496** 462

[30] Suryanarayana C 2001 *Prog. Mater. Sci.* **46** 1

[31] Keskinen J, Pogany A, Rubin J and Ruuskanen P 1995 *Mater. Sci. Eng. A* **196** 205

[32] Cullity B D 1969 *Elements of X-ray diffraction* (Reading, MA: Addison-Welsey)

[33] Forouzanmehr N, Karimzadeh F and Enayati M H 2009 *J. Alloys Compnd.* **471** 93

[34] Fadeeva V I, Leonov A V, Szewczak E and Matyja H 1998 *Mater. Sci. Eng. A* **242** 230

[35] Erschbaumer H, Podloucky R, Rogl P and Temnitschka G 1993 *Intermetallics* **1** 99

[36] Chang S Y 2007 *J. Mater. Eng. Perform.* **16** 508

[37] Reddy R G, Wen X and Divakar M 2001 *Metall. Mater. Trans. A* **32** 2357

[38] Vojtech D, Popela T, Kubasek J, Maixner J and Novak P 2011 *Intermetallics* **19** 493

[39] Schutze M and Hald M 1997 *Mater. Sci. Eng. A* **239–240** 847

[40] Perez P, Jimenez J A, Frommeyer G and Adeva P 2000 *Mater. Sci. Eng. A* **284** 138